



HAL
open science

An innovative calibration method for the inversion of satellite observations

Filipe Aires, Frédéric Bernardo, H el ene Brogniez, Catherine Prigent

► **To cite this version:**

Filipe Aires, Fr ed eric Bernardo, H el ene Brogniez, Catherine Prigent. An innovative calibration method for the inversion of satellite observations. *Journal of Applied Meteorology and Climatology*, 2010, 49 (12), pp.2458-2473. 10.1175/2010JAMC2435.1 . hal-00490363

HAL Id: hal-00490363

<https://hal.science/hal-00490363>

Submitted on 20 Nov 2020

HAL is a multi-disciplinary open access archive for the deposit and dissemination of scientific research documents, whether they are published or not. The documents may come from teaching and research institutions in France or abroad, or from public or private research centers.

L'archive ouverte pluridisciplinaire **HAL**, est destin ee au d ep ot et  a la diffusion de documents scientifiques de niveau recherche, publi es ou non,  emanant des  tablissements d'enseignement et de recherche fran ais ou  trangers, des laboratoires publics ou priv es.

An Innovative Calibration Method for the Inversion of Satellite Observations

FILIPÉ AIRES*

Laboratoire de Météorologie Dynamique/IPSL/CNRS, Université de Paris VI/Jussieu, and Laboratoire de l'Etude du Rayonnement et de la Matière en Astrophysique, CNRS, Observatoire de Paris, Paris, France

FRÉDÉRIC BERNARDO*

Laboratoire de Météorologie Dynamique/IPSL/CNRS, Université de Paris VI/Jussieu, Paris, France

HÉLÈNE BROGNIEZ

Laboratoire Atmosphères, Milieux, Observations Spatiales/IPSL/CNRS, Paris, France

CATHERINE PRIGENT

Laboratoire de l'Etude du Rayonnement et de la Matière en Astrophysique, CNRS, Observatoire de Paris, Paris, France

(Manuscript received 10 November 2009, in final form 18 May 2010)

ABSTRACT

Retrieval schemes often use two important components: 1) a radiative transfer model (RTM) inside the retrieval procedure or to construct the learning dataset for the training of the statistical retrieval algorithms and 2) a numerical weather prediction (NWP) model to provide a first guess or, again, to construct a learning dataset. This is particularly true in operational centers. As a consequence, any physical retrieval or similar method is limited by inaccuracies in the RTM and NWP models on which it is based. In this paper, a method for partially compensating for these errors as part of the sensor calibration is presented and evaluated. In general, RTM/NWP errors are minimized as best as possible prior to the training of the retrieval method, and then tolerated. The proposed method reduces these unknown and generally nonlinear residual errors by training a separate preprocessing neural network (NN) to produce calibrated radiances from real satellite data that approximate those radiances produced by the “flawed” NWP and RTM models. The final “compensated/flawed” retrieval assures better internal consistency of the retrieval procedure and then produces more accurate results. To the authors’ knowledge, this type of NN model has not been used yet for this purpose. The calibration approach is illustrated here on one particular application: the retrieval of atmospheric water vapor from the Advanced Microwave Scanning Radiometer for Earth Observing System (AMSR-E) and the Humidity Sounder for Brazil (HSB) measurements for nonprecipitating scenes, over land and ocean. Before being inverted, the real observations are “projected” into the space of the RTM simulation space from which the retrieval is designed. Validation of results is performed with radiosonde measurements and NWP analysis departures. This study shows that the NN calibration of the AMSR-E/HSB observations improves water vapor inversion, over ocean and land, for both clear and cloudy situations. The NN calibration is efficient and very general, being applicable to a large variety of problems. The nonlinearity of the NN allows for the calibration procedure to be state dependent and adaptable to specific cases (e.g., the same correction will not be applied to medium-range measurement and to extreme conditions). Its multivariate nature allows for a full exploitation of the complex correlation structure among the instrument channels, making the calibration of each single channel more robust. The procedure would make it possible to project the satellite observations in a reference observational space defined by radiosonde measurements, RTM simulations, or other instrument observational space.

* Current affiliation: Estellus, S.A.S., Paris, France.

Corresponding author address: F. Aires, Estellus, LERMA/Observatoire de Paris, 61 avenue de l’Observatoire, 75014 Paris, France.
E-mail: filipe.aires@estellus.fr

1. Introduction

In the context of satellite remote sensing, calibration often refers to the quantification and the adjustment of the instrument responses to known signals that are traceable to agreed standard. This is a very general definition: one dataset is transformed so that it becomes closer, in some sense that needs to be specified, to a reference dataset. This definition covers a large ensemble of applications: to adjust the response of an instrument, to correct the instrument's drift over time, or to intercalibrate multiple instruments. This paper concentrates on the "inversion for calibration," which deals with the transformation of the satellite observations to improve the retrieval process. However, the methodology presented in this study is very general and this introduction mentions various aspects of calibration.

A reliable instrument calibration is a prerequisite for any retrieval scheme. The calibration has to be stable over a long time period and free from any biases. This is a difficult task because the satellite observations can be polluted by an instrument drift plus a legitimate climatological trend. Colton and Poe (1999) performed significant intercalibration work on the series of Special Sensor Microwave Imager (SSM/I) microwave instruments. Even if only one type of instrument is involved, satellite drift within the lifespan of one given satellite and satellite intercalibration between successive satellites of the same family can be very difficult to achieve. The analysis of the Normalized Difference Vegetation Index (NDVI) from the Advanced Very High Resolution Radiometer (AVHRR) over long time series suffers from these difficulties (Gutman 1999). In addition, when trying to cover the whole globe and the full diurnal cycle, the simultaneous use of several satellite types is necessary and stringent constraints are then imposed on the satellite intercalibration. For instance, the International Satellite Cloud Climatology Project (ISCCP; Rossow and Schiffer 1999), which supplies global cloud information every 3 h, combines all the visible and infrared observations from the National Oceanic and Atmospheric Administration (NOAA) polar orbiters and the geostationary satellites to provide both the spatial and temporal coverages. A huge effort has been dedicated to the accurate radiance calibration and intercalibration of all the instruments over the long time series to produce the ISCCP results (Brest et al. 1997). Another example is provided by the long-term study of the upper-tropospheric humidity variability estimated from measurements derived from geostationary satellites such as the Meteosat series. For this purpose, it is necessary to correct for the heterogeneities induced by 1) the successive radiometers with slightly different filter functions and 2) the

improvement of the vicarious calibration techniques used by the European Organisation for the Exploitation of Meteorological Satellites (EUMETSAT; Picon et al. 2003; Brogniez et al. 2006).

In addition to a detailed and systematic analysis of each sensor calibration from an engineering point of view, various methodologies have to be developed to calibrate the satellite observations in order to improve the retrievals. For example, if multiparameter retrievals are performed using multiple satellite observations, the calibration of the instruments needs to be consistent at several levels. First, the calibration has to be consistent among the various channels of a given instrument. From the point of view of information theory, it is not optimal to calibrate independently the various channels (essentially by monitoring the mean and standard deviation over time or by indirect comparison with in situ measurements). The covariance among channels can be exploited to perform the calibration and this potential should be examined. At least, monitoring the interdependence among the channels can help check the calibration quality. However, caution has to be exercised in this procedure since too stringent constraints could mask some real extreme behavior in one channel. Second, the inter-satellite calibration has to be performed and consistency has to be ensured across platforms. Observations from coincident overpasses can be compared, provided that the measurements are performed exactly in the same conditions (frequency, incidence angle, polarization). An alternative is to compare the retrieved products from the two coincident satellite measurements. Rigorous statistical comparisons of radiative transfer model (RTM) calculations and satellite observations can also be performed, with the same assumptions for the two satellites, in order to diagnose the radiance biases between instruments. The retrieved products across satellites can also be compared.

A generic calibration method that includes many of these above aspects is under development at NOAA/National Environmental Satellite, Data, and Information Service (NESDIS) to intercalibrate radiometers in the visible, infrared, and microwave (Weng et al. 2005). It has already been applied to Microwave Sounding Unit (MSU) (Zou et al. 2006, 2009). In the Global Precipitation Mission (GPM) framework, efforts are also conducted to intercalibrate the passive microwave imagers on a common standard to ensure consistency among precipitation products (C. Kummerow 2009, personal communication; see <http://mrain.atmos.colostate.edu/LEVEL1C/index.html>).

Having together all the satellite observations and using the same methods and data to calibrate them would inevitably benefit the retrieval. For instance, it is worrying

to realize that there is not one uniformly calibrated set of the Scanning Multichannel Microwave Radiometer (SMMR) and SSM/I observations over the full period of satellite operation that is easily available to the user community. A strong effort should be supported to systematically apply these new calibration approaches. The resulting multiplatform calibrated datasets should be easily accessible to the community: it would stimulate the developments of the next generation of retrieval algorithms.

Modern satellite applications are involving an increasing number of measurements from various instruments and platforms. The use of multiple sources of information in a unique algorithm [such as in an assimilation scheme in a numerical weather prediction (NWP) center] requires the observations to be coherent. For example, the European Centre for Medium-Range Weather Forecasts (ECMWF) assimilates the satellite observations from a large set of instruments. To assimilate all these observations, a particular calibration scheme has been developed. However, this calibration is specifically designed for the ECMWF assimilation scheme. The calibration is part of the assimilation process itself: the calibration coefficients evolve with time and space to force the agreement between the model and the satellite observations. This means that this calibration effort cannot be directly used in other contexts.

Any physical retrieval scheme or equivalent method uses, explicitly or implicitly, 1) an RTM inside the retrieval procedure (e.g., iterative inversion) or to construct the learning dataset used to calibrate the statistical retrieval algorithms, and 2) an NWP model to provide a first guess or, again, to construct a learning dataset. This is particularly true in operational centers. As a consequence, any physical retrieval or similar method is limited by inaccuracies in the RTM and NWP models on which it is based. In this paper, a method for partially compensating for these errors as part of the sensor calibration is presented and evaluated. In general RTM/NWP errors are minimized as best as possible prior to the training of the retrieval method, and then tolerated. The proposed method reduces these unknown and generally nonlinear residual errors: it trains a separate preprocessing neural network (NN) to produce calibrated radiances from real satellite data that approximate those radiances produced by the “flawed” NWP and RTM models. Having thus tuned the observed radiances to be more consistent with the flawed training of the retrieval method, the final “compensated/flawed” retrieval assures better internal consistency of the retrieval procedure and produces more accurate results for those cases that are otherwise limited by NWP and RTM errors.

In this study, a water vapor (WV) retrieval scheme is developed for the *Aqua* platform using the Advanced

Microwave Scanning Radiometer for Earth Observing System (AMSR-E) and the Humidity Sounder for Brazil (HSB) instruments. This inversion algorithm is designed by training an NN on a learning dataset built from RTM simulations over one year of operational analysis from ECMWF. For internal consistency, when used on real satellite observations, this retrieval scheme requires the calibration of the observations onto the space of the RTM simulations. It will be shown that the retrieval of WV is improved when using our calibration procedure before the inversion algorithm is applied.

The datasets used in this study are presented in section 2. Section 3 introduces the calibration methodology and results. The impact of the calibration procedure on a WV retrieval algorithm is discussed in section 4. Section 5 provides a discussion on some perspectives of the calibration methodology. Conclusions are drawn in section 6.

2. Datasets

This study focuses on clear and nonprecipitating atmospheric situations over both land and ocean.

The dataset used as a “reference” for the projection of the actual satellite observations could be a large sample of in situ measurements from radiosondes. First, these radiosondes are not uniformly distributed over the globe. Second, they can require significant quality control and interpolation/extrapolation work to be used as inputs to RTM simulations. Third, the number of coincident radiosondes can be limited if just few months of real observations are available, which is the case for this experiment.

Instead, RTM simulations performed on the analysis from the ECMWF model are used here as the reference dataset. Such a dataset avoids the previously mentioned limitations of the radiosondes. Furthermore, the horizontal and vertical resolution of the analysis is compatible and appropriate for climate models, which is a strong advantage for a possible forthcoming variational assimilation.

To compare real satellite observations and RTM simulations, several datasets need to be put in space/time coincidences.

a. AMSR-E/HSB observations

The satellite measurements are composed of collocated observations from two microwave radiometers onboard the *Aqua* platform, AMSR-E and HSB (HSB only operated from May 2002 to February 2003). AMSR-E is a dual-polarized radiometer observing at 6.9, 10.7, 18.7, 23.8, 36.5, and 89 GHz. The instrument has

a conically scanning antenna that provides multichannel observations at a constant incidence angle of 55° across a 1445-km swath. The spatial resolution of AMSR-E varies from approximately 60 km at 6.9 GHz to 5 km at 89 GHz (Kawanishi et al. 2003). The HSB cross-track sounder is a nearly identical copy of the Advanced Microwave Sounding Unit B (AMSU-B) with four moisture sounding channels (instead of five for AMSU-B). Three out of four are located around the strong water vapor absorption line at 183.31 GHz (± 1.0 , ± 3.0 , and ± 7.0) and the fourth channel is a window channel at 150 GHz that measures part of the water vapor continuum (Lambertsen and Calheiros 2003). During one scan, HSB samples ninety 1.1° scenes, from -49.5° to $+49.5^\circ$, with a footprint size of 13.5 km at nadir. The 12 channels of AMSR-E coupled to the four channels of HSB provide a monitoring of the earth's water cycle: profiles of atmospheric water vapor, cloud water, precipitation rate, sea surface winds and temperature, soil moisture, snow water equivalent, and sea ice concentration.

The collocation between AMSR-E and HSB footprints assumes that for both sensors, the footprints are coregistered. Observations for AMSR-E are extracted from level-2A data that provide a resampling of the nominal resolution observations into coarser-resolution fields of view. In the present study, the chosen resolution is 21 km. The coastal pixels are suppressed. HSB observations are taken from level-1B data (calibrated, geolocated, and scene analyzed). The collocation method averages all the HSB scenes that fall into each AMSR-E elliptical footprint, at a maximum time difference of 70 s and assuming that the information provided for each HSB scene is concentrated at its center. The final satellite database is composed of two full months of observations (September 2002 and January 2003) containing the 16 collocated brightness temperatures, plus the land fraction information provided by the HSB data.

b. ECMWF operational analyses

In addition to the satellite database described in section 2a, a dataset of surface and atmospheric situations is built up: they will be used by the RTM model to simulate the satellite responses and compare them to the satellite real observations. Hence, we use atmospheric profiles and surface properties from the 6-hourly operational global analyses from the Integrated Forecasting System (IFS) of the ECMWF provided on a regular 1.125° grid (hereinafter referred to as the ANA database). To run the most accurate RTM simulations, the following information is kept: the temperature, water vapor and ozone profiles on 21 pressure levels ranging from 1000 to 1 hPa, the cloud profiles (cloud cover and liquid and ice water) on the 60 nominal model levels, and surface

properties (10-m horizontal wind, 2-m pressure and temperature, surface temperature, convective and large-scale precipitation, and total cloud cover).

In the following, only nonprecipitating situations are considered to avoid possible biases in the simulation due to the scattering of the upwelling radiation by droplets: a threshold of $\frac{1}{6} \text{ mm h}^{-1}$ in the precipitation fields is adopted. Furthermore, scenes above 1000 m in altitude are discarded to limit topography effects.

The AMSR-E/HSB observations and the ANA database are collocated in time ($\Delta t = 3 \text{ h}$) and space (nearest-neighbor, no averaging), over the $\pm 30^\circ$ latitude band. Over the 2-month period, this results in a coincident database of more than 1 million points over sea and land.

c. A global land surface microwave emissivity dataset

For atmospheric profiling, surface-sensitive microwave observations are so far essentially used over ocean. Over land, the surface emissivity is difficult to estimate: it is usually high, limiting the contrast with the atmospheric contribution, very variable in space, and complex to model.

A parameterization of the land surface microwave emissivities has been recently developed (Prigent et al. 2008). For each location and time of the year, it provides realistic first-guess estimates of the land surface microwave emissivities from 19 to 100 GHz for all scanning conditions, incidence angles, and polarizations. It is anchored to climatological monthly-mean maps of the emissivities at 19, 37, and 85 GHz, calculated from SSM/I (Prigent et al. 1997, 2006). It is originally designed for frequencies between 19 and 85 GHz but tests proved that it is beneficial down to 5 GHz and up to 190 GHz. The nominal spatial resolution of the emissivity estimates is $0.25^\circ \times 0.25^\circ$. The results have been thoroughly evaluated and the root-mean-square (RMS) errors are usually within 0.02, with the noticeable exception of snow-covered regions where the high spatial and temporal variability of the emissivity signatures are difficult to capture. A tool based on this parameterization is under development for the EUMETSAT NWP Satellite Application Facility (SAF) (Aires et al. 2009, manuscript submitted to *Quart J. Roy. Meteor. Soc.*). Figure 1 shows the emissivity atlas at 85 GHz for the horizontal polarization for September 2002 at 0.25° .

d. The RTTOV radiative transfer simulations

The Radiative Transfer for Television and Infrared Observation Satellite (TIROS) Operational Vertical Sounder (RTTOV)-9.3 RTM is used to simulate the AMSR-E and HSB instruments. This model, originally developed at ECMWF (Eyre 1991) and now supported by the EUMETSAT NWP SAF (Saunders et al. 1999;

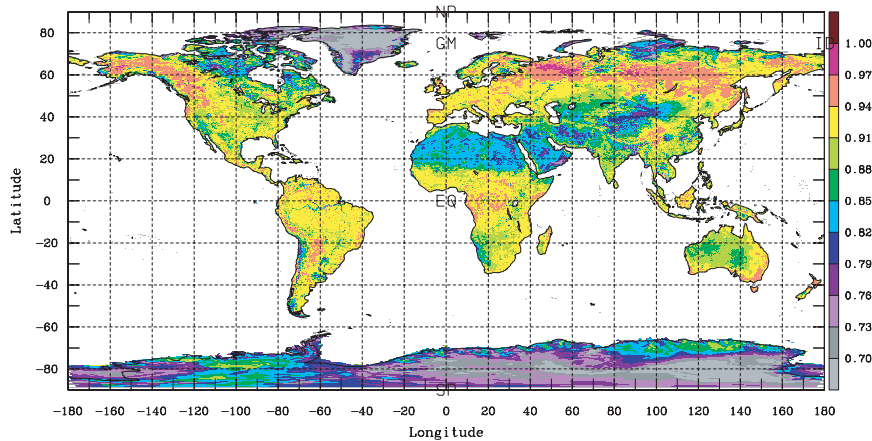


FIG. 1. Emissivity at 85 GHz (horizontal polarization) for September 2002.

Matricardi et al. 2001), allows for rapid simulations of radiances for satellite infrared and microwave radiometers for a given atmospheric state vector.

To compare real satellite observations and RTM simulations, RTTOV is run using all the ANA information (section 3b) together with the surface emissivities database over land (section 3c), while over ocean the emissivities are computed by the Fast Emissivity Model, version 3 (FASTEM-3; Deblonde and English 2001), surface model. To keep the spatial variability of the land surface emissivities (see Fig. 1), all the pixels of the 0.25° emissivity database are associated to its closest ANA 1.125° grid point. In other words, over continental areas one atmosphere of the ANA database is reproduced for multiple different values of emissivities. Based on these inputs parameters, RTTOV is used to perform simulations of AMSR-E and HSB brightness temperatures (TBs). These simulated TBs are compared with the coincident real observations, described in section 3a.

e. Radiosonde measurements

To check the quality of the retrievals compared to the ECMWF analysis, the September 2002 and January 2003 radiosondes are extracted from the ECMWF operational sounding archive used during the assimilation process in the 40-yr and interim ECMWF reanalyses (ERA-40 and ERA-Interim; Uppala et al. 2005). The temperature and humidity measurements have been quality-controlled in order to discard incomplete profiles (threshold of 30 hPa for the temperature and 350 hPa for the humidity), and a vertical extrapolation was applied up to the top of the atmosphere (5.10–2 hPa) using a climatology [R. Armante, Laboratoire de Météorologie Dynamique (LMD), 2008, personal communication]. Finally,

the measurements are interpolated on a fixed 40-level pressure grid.

3. Calibration procedure and results

In this section, we present a novel approach to “calibrate” one dataset to another. The calibration can be seen as a statistical problem: How can measurements in one data space be transformed to become statistically “closer” (in a sense that needs to be specified) to another data space? This definition, very general on purpose, covers a large ensemble of applications.

Many statistical retrieval schemes use a statistical dataset to calibrate their inversions. This dataset is very often constructed using RTM simulations. Then, the inversion algorithm should be applied to data that are coherent with the simulations used to calibrate it: Real observations from *Aqua* need to be calibrated to the simulation space so that the inversion scheme is coherent.¹ For demonstration purposes, the calibration method is applied to one particular case: the retrieval of atmospheric WV from AMSR-E/HSB *Aqua* measurements.

a. NN calibration model

NNs have been widely used to perform nonlinear transformations from one space to another, by following some particular statistical constraints. In particular, NN techniques have been very successful in developing computationally efficient algorithms for remote sensing applications. For example, an NN algorithm is applied to retrieve simultaneously the atmospheric temperature and

¹ In some contexts, it is also possible that the simulated dataset needs to be “calibrated” to real observations.

humidity atmospheric profiles at 23 fixed pressure levels from 1000 to 1 hPa over sea using AMSU-A and -B observations (Aires and Prigent 2007). In this study, we propose to use such NNs to calibrate satellite observations. The NN model is a classical architecture but the use of this type of model for calibration as a pre-processing step before inversion is, to our knowledge, novel.

The multilayered perceptron (MLP) model (Rumelhart et al. 1986) is the NN model that is selected here. It is a nonlinear mapping model: given an input X , it provides an output Y in a nonlinear way. The complexity captured by MLPs is strongly limited in practice by the fact that backpropagation training of NNs is nondeterministic polynomial time (NP)-complete (Blum and Rivest 1992) and by their need for enormous unbiased training sets as complexity increases. As often occurs in satellite applications, the number of samples is not an issue in this study. The limiting factor is often the information content of the satellite observations. In our case, X is composed of the data to be calibrated and Y represents the calibrated data. We illustrate the methodology using AMSR-E/HSB observations. The dimension of inputs and outputs is dictated by the problem; the network architecture is defined by the number of hidden layers and the number of neurons in the hidden layer(s). The architecture of the NN has 16 neurons in the input layer (i.e., the 16 observed TBs), 10 neurons in the hidden layer, and 16 neurons in the output layer (i.e., the 16 calibrated TBs). The optimization of the number of hidden neurons is performed using a heuristic approach but the learning is performed on a training dataset and the capacities of the NN are tested on an independent dataset in order to avoid overtraining/overparameterization problems.

b. Learning dataset

The NN is trained to reproduce the behavior described by a database of samples, that is, the learning dataset, composed of inputs X^e (i.e., the real observations TBs) and their associated outputs Y^e (i.e., the calibrated TB), for $e = 1, \dots, N$, with N being the sample's number in the learning database. Provided that enough samples (X^e, Y^e) are available (usually the case in satellite applications), any continuous relationship, as complex as it is, can be represented by an MLP (Hornik et al. 1989; Cybenko 1989).

The real AMSR-E/HSB observations from the *Aqua* platform and the respective TB RT-TOV simulations presented in section 2 constitute here the learning dataset. The NN is designed to “project” or calibrate the actual real *Aqua* observations into the space of the RTTOV simulations.

The quality of the learning dataset is essential for the final NN performance. The learning dataset includes some sources of errors that need to be mentioned:

- errors of the ECMWF analysis (geophysical variables at the surface or the atmosphere from the analysis can have errors that impact the RTM simulations),
- coincidence errors in time and space between ECMWF analysis and real satellite observations,
- errors due to the difference on the spatial resolution of the analysis and satellite data, and
- imperfections of the RTM code resulting in systematic bias or RMS errors.

The goal of the calibration procedure is to reduce the NWP and RTM errors (e.g., bias, range of variability, structure, saturations) inside the calibration procedure, but it should be kept in mind that other sources of discrepancies are still present in the learning database and that the calibration procedure cannot suppress them by building a perfect bridge between real and simulated satellite TBs.

Four NNs have been derived, for cloud-free and cloudy situations, and for land and ocean scenes. The cloud flag is derived from the ECMWF reanalysis.² We are aware of the uncertainty with this variable, but it nevertheless makes it possible to separate the analysis in two broad classes, with different sensitivities to the parameters. For the learning of these NNs, four different learning databases have been constructed:

- cloud-free-over-ocean scenes (CF/O),
- cloud-free-over-land scenes (CF/L),
- cloudy-over-ocean scenes (CL/O), and
- cloudy-over-land scenes (CL/L).

Each one of these four learning datasets includes about 100 000 situations, which is largely sufficient to train the four respective NNs. Two particular months of data have been used to generate these learning databases (section 2), but in an operational context the learning dataset could be regularly updated with the most recent satellite observations. In this way, the calibration procedure would become adaptive, which means that its properties evolve in real time.

c. Comparison of real and simulated satellite observations

The first measure of discrepancies between two datasets is the bias (i.e., the systematic difference of the two datasets). This bias can be a very important problem if the retrieval scheme uses the absolute values of the

² Tests are under way to develop a cloud classification scheme based on the MW satellite observations.

observations. If only relative values are required, then it is not a problem. There is generally some bias between real and simulated satellite observations. Good statistical samples allow for the estimation of these systematic differences. These biases are given in Table 1. The suppression of these biases from the real observations is the first stage of the calibration procedure introduced in this paper. Bigger errors seem to be related to the surface, especially for horizontally polarized channels that have a larger variability of their emissivities. We can also note that the larger errors occur below 18 GHz for channels where we had to interpolate the surface emissivity (see section 2c).

The RMS of the differences between simulated TBs and calibrated or noncalibrated real observations are represented in Fig. 2 for the four configurations (CF/O, CF/L, CL/O, and CL/L). All the situations where the difference between the simulated and observed TBs is larger than 40 K are filtered out: these situations likely correspond to nonfiltered precipitating scenes (section 3b). The impact of the calibration can be directly measured by comparing the solid (calibrated) and dashed (noncalibrated) lines. It is interesting to see that the calibration often reduces the discrepancies between simulated and observed satellite measurements by a few kelvins. This is true for land scenes, for both cloud-free and cloudy situations, and for all channels for both AMSR-E and HSB instruments. For ocean scenes, the improvement is also significant for cloud-free and cloudy situations, except for 18.7 and 23.8 GHz for clear scenes, where the impact is slightly negative.

Other statistical results were analyzed (not shown) to check the quality of the calibration: 1) error distributions are less spread when using the calibrated data, 2) correlation levels between channels are only slightly increased when the observations are calibrated, and 3) the scatterplots of differences showed that the quality of the calibration procedure is satisfactory for all ranges of brightness temperatures.

In Fig. 3, maps of RMS errors are represented for differences between simulations and the (left) raw or (right) calibrated observations. Statistics are performed over the two months of data (see section 3b) for (top) HSB channel 183.31 ± 1 GHz and (bottom) AMSR-E channel 18.7 GHz, horizontal polarization. This figure includes the four separate configurations that the calibration procedure deals with: over land and ocean surfaces and for clear and cloudy (but nonprecipitating) scenes. It can be seen that the errors decrease from left to right, meaning that the calibration reduces differences between simulations and observations.

Furthermore, statistics have been performed to test the angle dependency of these results (not shown). No

TABLE 1. Bias statistics [simulations (sim) – real observations] between RTTOV TB simulations and real observations from AMSR-E and HSB on board the *Aqua* platform. The ECMWF analyses are used as input for the RTM simulations. The characteristics of the instrument noises are also indicated for each channel.

			Bias (K) (sim – real obs)			
			Clear		Cloudy	
	Freq. (GHz)	Noise (K)	Land	Ocean	Land	Ocean
AMSR-E	6.9 V	0.3	–2.71	–2.67	1.07	–1.39
	6.9 H	0.3	8.43	–2.60	7.79	–0.47
	10.8 V	0.6	–1.70	–1.71	1.45	–0.64
	10.8 H	0.6	6.25	–1.40	5.62	0.53
	18.7 V	0.6	–2.85	–0.77	0.47	2.96
	18.7 H	0.6	0.23	0.14	1.97	6.77
	23.8 V	0.6	–2.93	–0.20	0.48	4.06
	23.8H	0.6	–0.02	0.82	2.37	8.44
	36.5 V	0.6	–4.78	–0.63	–0.88	3.70
	36.5 H	0.6	–1.75	–1.47	1.11	7.09
	89.0 V	1.1	–7.00	–2.60	–4.21	0.24
	89.0 H	1.1	–5.27	–6.00	–2.81	2.39
	HSB	150.0	1.0	–4.00	–1.57	–2.16
183.311 ± 1		1.0	–1.13	–1.13	0.14	–0.41
183.311 ± 3		1.0	–0.75	–0.72	1.30	0.11
183.311 ± 7		1.2	–0.83	–0.20	–1.85	–1.11

angle dependency was found, so the final calibration procedure does not take into account the scanning angle information.

In the following, the impact of the calibration procedure is measured on the quality of the WV retrieval.

4. Calibration impact on water vapor retrieval

The inversion scheme is not presented here thoroughly (it will be the subject of another study). The WV inversion is used only to evaluate the impact of the calibration scheme. The quality of the WV retrievals will be assessed on both the relative humidity and brightness temperature spaces.

a. WV retrieval scheme

The retrieval scheme is composed of an MLP neural network, similar to the NN described in section 3a for the calibration. The inputs are the 16 observations from *Aqua* over ocean, plus 16 microwave surface emissivity first guesses over land. There are 44 outputs over ocean: the 43 WV contents of the atmospheric profile layers from the surface to the top of the atmosphere and the surface wind speed. Over land, there are 60 outputs: the 43 WV contents plus the surface temperature and the 16 emissivities. Hence, the network architecture has 16 (32) neurons in the input layer for the ocean (land) case. It has 44 (60) neurons in the output layer over ocean (land). The number of neurons in the hidden layer is optimized by

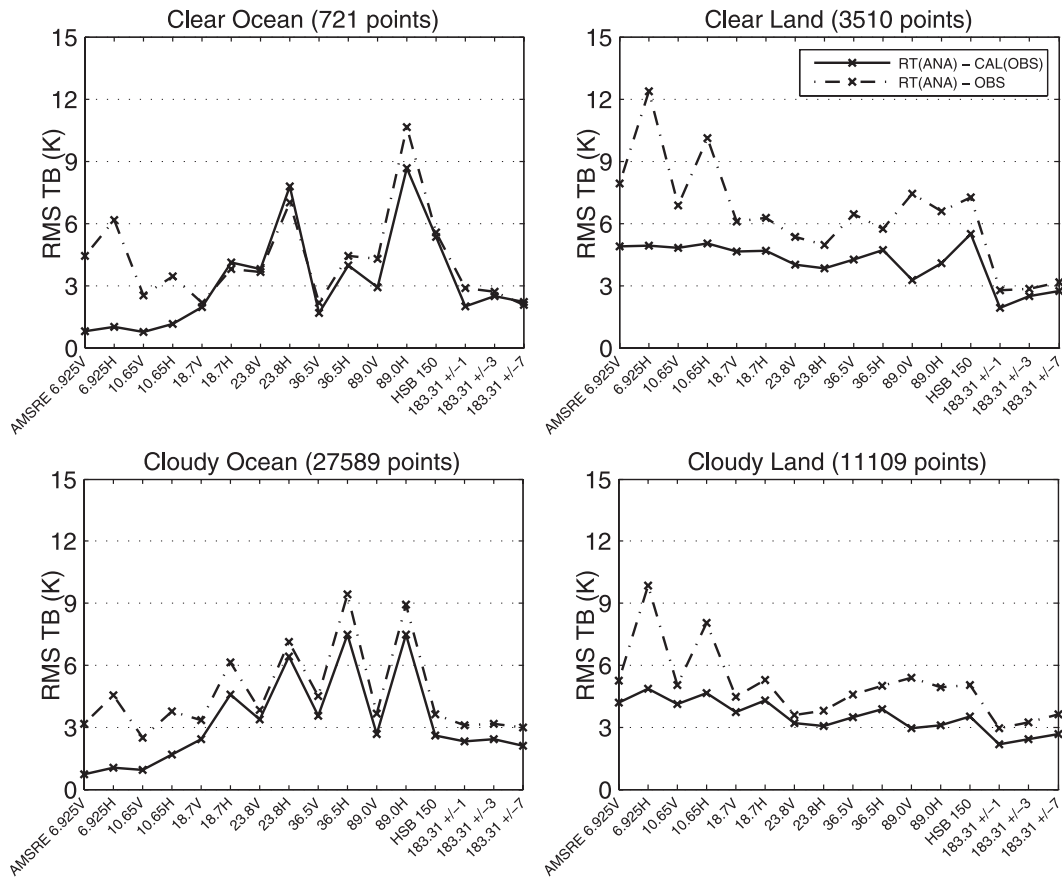


FIG. 2. RMS differences between observed and calibrated data for AMSR-E and HSB channels. Four cases are considered: (top) cloud free and (bottom) cloudy without precipitation, for (left) ocean and (right) land scenes. The solid and dashed lines correspond to the RMS difference when using calibrated and noncalibrated TBs, respectively.

trial and error and finally set to 30. As for the calibration procedure, four NNs have been derived, for cloud-free and cloudy situations and for land and ocean scenes.

In this study, no a priori information on the WV profile is used by the retrieval. It would be possible to use a priori information in an NN retrieval scheme (Aires et al. 2001), but the ANA WV is already very good because all the satellite observations available in the NWP centers and all the radiosondes from the Global Transmission System have been assimilated. By using WV a priori information in the retrieval scheme, it would have been difficult to measure the information content of the actual satellite observations.

To train the NN, two strategies could be used:

- The training could be performed on a learning database composed of real *Aqua* observations and collocated WV profiles from ECMWF analysis. This type of scheme is said to be an “empirical” inversion because no RTM is used to solve the inverse problem.
- The inversion can also be trained on a learning database composed of the same WV profiles from ECMWF

analysis, but with *Aqua* satellite observations (from AMSR-E and HSB instruments) simulated by a RTM coupled to atmospheric profiles instead of real observations directly. This type of inversion is said to be a “physical” inversion.

The scheme in Fig. 4 illustrates these two options. The first approach involves only one transformation of the real observations: It mixes the calibration and the retrieval in a unique procedure. The second approach explicitly involves two transformations, namely the calibration of the data and the actual retrieval. Both methods could lead to similar results, but the second one is preferred here for multiple reasons. First, it is always a good idea to control the quality, defaults, and uncertainties associated with each step of a processing chain. Knowing the difficulties provides ways of improvement and defines the application limit of the method. Second, if the instruments evolve with time, the calibration also needs to evolve. It is simpler to have this calibration changing over time independently of the nonevolving retrieval step. Finally, this calibration technique for satellite data is very general

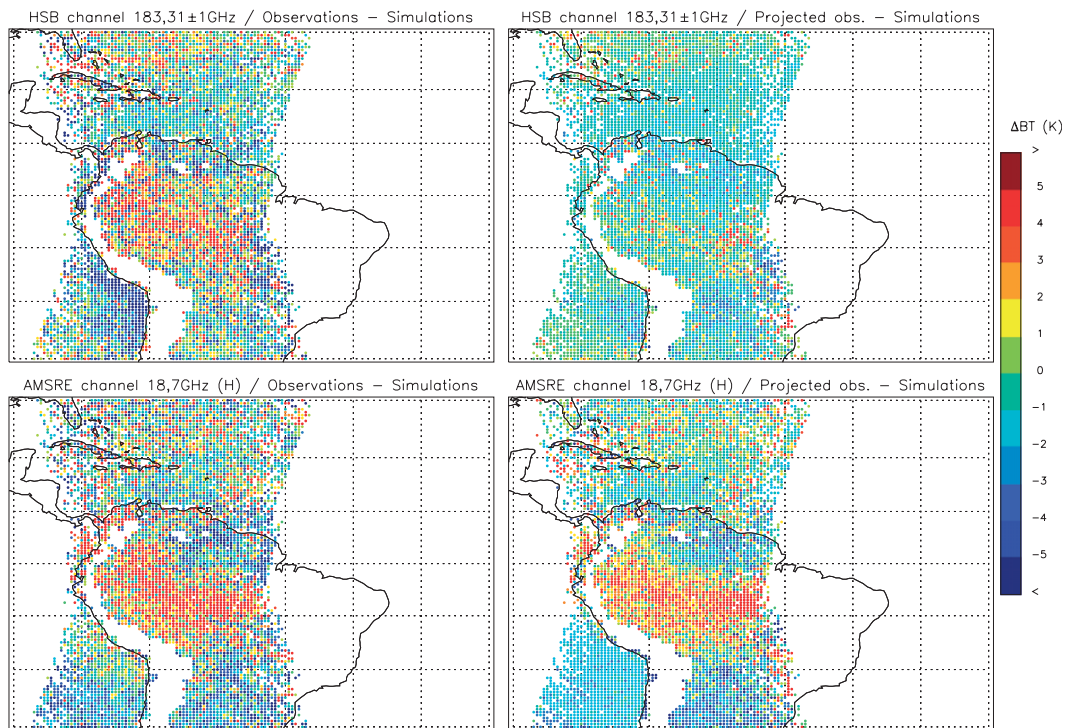


FIG. 3. RMS error maps computed over two months for differences between RTTOV simulations and (left) real *Aqua* observations and (right) calibrated *Aqua* observations for (top) an HSB channel at 183.31 ± 1 GHz and (bottom) an AMSR-E channel at 18.7 GHz, vertically polarized.

and shows the potential of the technique for very different applications.

The learning dataset is composed of atmospheric situations sampled over one year of ECMWF analysis (section 2b), and all the variables necessary to feed a RTM are kept. The RTTOV model (section 2d) is used to simulate satellite observations at AMSR-E and HSB frequencies. The instrument noise of the *Aqua* instruments (Table 1) is taken into account in the training process.

b. Evaluation of the calibration

Two general retrieval strategies are generally considered: the so-called empirical retrieval schemes have a “learning” dataset of coincident satellite measurements and realistic WV profiles. In this case, no RTM is involved and a statistical procedure is used to model the link between the observations and the WV. The second type of retrieval scheme uses a RTM; this is the approach adopted in this paper. Empirical retrieval schemes can be used if no RTM is satisfactory or if the dataset of geophysical variables (i.e., the WV profile) is particularly good. On the contrary, the physical retrieval schemes rely on the RTM ability to simulate realistic satellite observations.

In empirical retrieval schemes, the inversion algorithm has to retrieve WV profiles as close as possible to

the realistic WV profiles included in the learning dataset. With physical algorithms, the inversion algorithm has to estimate WV profiles that, when used as RTM input, provide simulated satellite observations that are as close as possible to the actual real observations. As a consequence, it is important for the “physical” retrieval scheme presented in this study to check the retrievals in the space of the WV profiles (comparisons with ECMWF analysis and radiosondes) but, most importantly, to test them also in the space of the satellite observations themselves.

1) DEPARTURE FROM THE ECMWF ANALYSES

Figure 5 represents the RMS of the departure of the retrieval from the ECMWF analysis, over the two months over the tropics and for six atmospheric layers.³ Calibration

³ It has been explained previously that the WV retrieval was performed on 43 atmospheric layers. AMSR-E and HSB instruments cannot provide such high vertical resolution. The choice of retrieving the WV profile on that many atmospheric layers was made for practical considerations: In particular, it allows for direct RTTOV simulations on the WV profile. However, the actual real retrieval of our inversion scheme is defined on six thicker layers delimited by the surface, 920, 750, 560, 400, 250 hPa, and the top of the atmosphere. This choice has been analyzed and optimized to limit the retrieval errors in the atmospheric layers.

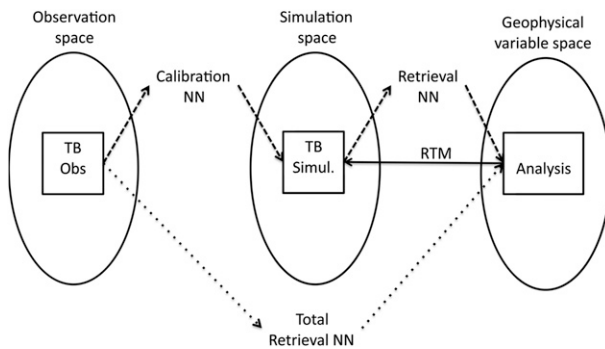


FIG. 4. Schematic representation of the observations, simulated TBs, and geophysical spaces together with the various links/relationships investigated in this study. Two strategies can be used to perform the WV retrieval from the “TB Obs” space to the “Geophysical variable” space. The first is a “Total Retrieval NN” (dotted arrows) that performs at the same time the calibration and the retrieval. In this case, the TB Obs and the analysis are put in coincidence and this dataset is used to train the retrieval scheme. In the second case—see the two NNs (dashed arrows) with an intermediate step in the “TB Simul” space—an NN calibration is trained to link TB Obs and TB Simul: the learning dataset is constituted of the coincidence of real observations, TB Obs, and simulations performed in the analysis, TB Simul. The second NN links the TB Simul to the Analysis; this is a classical retrieval trained on a synthetic dataset. The RTM arrow represents the relationship $TB\ Simul = RTM(Analysis)$.

seems to degrade the statistics over ocean above 600 mb; the explanation for this behavior is that relative humidity becomes small at these levels and that the information content is very limited since weighting functions do not reach these altitudes. However, these departures cannot be directly considered as errors because it cannot be said a priori which one is the closest to reality: even if the ECMWF analysis is of good quality, the *Aqua* retrieval can be closer to reality at the higher spatial resolution of the satellite. The purpose of this figure is to show that the retrieval from calibrated data is closer to the ANA data than the retrieval without calibration, for most atmospheric layers. This is especially true in the lower atmosphere for the clear-sky situations over land. These results are not a proof that the retrieval is good but do show that the calibration procedure helps the retrieval of the WV profiles.

2) COMPARISON WITH RADIOSONDES

To measure the impact of the calibration on the quality of the WV scheme, the retrievals based on raw and calibrated *Aqua* observations are compared to about 500 radiosonde measurements, over land. Figure 6 represents the RMS differences. It is clear in this figure that the retrievals from calibrated *Aqua* observations (solid lines) are closer to radiosondes than the retrievals from raw

Aqua observations (dot-dashed lines). This is particularly true for the lower atmospheric layers (from 750 hPa down to the surface), with a decrease of the error of 5% close to the surface, which represents $\frac{1}{4}$ of the error under clear-sky conditions. This figure illustrates the main point of this paper: the calibration of the observations helps when the NWP/RTM models have errors and when satellite observations do add information.

The agreement between retrieved WV profiles and radiosondes is comparable to the agreement between the ANA and radiosondes (not shown). The statistics on the latter are slightly better, which is understandable since the ECMWF analysis assimilates the radiosondes.

c. Brightness temperature comparisons between retrievals from raw and calibrated data

It has been noted in the introduction of section 4b that for “physical” retrieval schemes, the quality criterion of the inversion process is based on the difference between the actual observations and RTM simulations. This quality criterion should be improved when the first guess or the a priori information on the state of the atmosphere is replaced by the retrieval. As a consequence, it is very natural to test the quality of a retrieval by checking the differences between RTM simulations and actual satellite observations. If the retrieval process degrades these statistics, the inversion has not improved the a priori or has mathematically diverged and failed to perform the retrieval.

The procedure used to validate the retrievals in the satellite observation space is described in Fig. 7, and the meaning of each component in this validation scheme is provided in Table 2. The observations (Fig. 7, top) can be directly inverted, $INV(obs)$ (Fig. 7, left), or they can be calibrated and then inverted, $INV[CAL(obs)]$ (Fig. 7, middle). All the geophysical variables retrieved by the inversion scheme described in section 4a are used as inputs for the RTM (i.e., RTTOV): the WV profile but also the surface temperature and emissivities over land, and the wind at the surface over ocean. The RTM simulations are performed on the noncalibrated inversions, $RT[INV(obs)]$ (Fig. 7, left), or on the calibrated inversions, $RT\{INV[CAL(obs)]\}$ (Fig. 7, middle). The RTM simulations are also performed using the raw ECMWF analysis (Fig. 7, right). The differences between the simulations on the analysis and the RTM simulations on inversions appear uniquely in the parameters that the inversion scheme retrieves, with all other parameters remaining identical. Comparisons in the TB space are represented in this scheme by colors (as in Fig. 8; see explanation directly below). Comparisons can be made between the three RTM simulations (Fig. 7, bottom) and the observations or the calibrated observations.

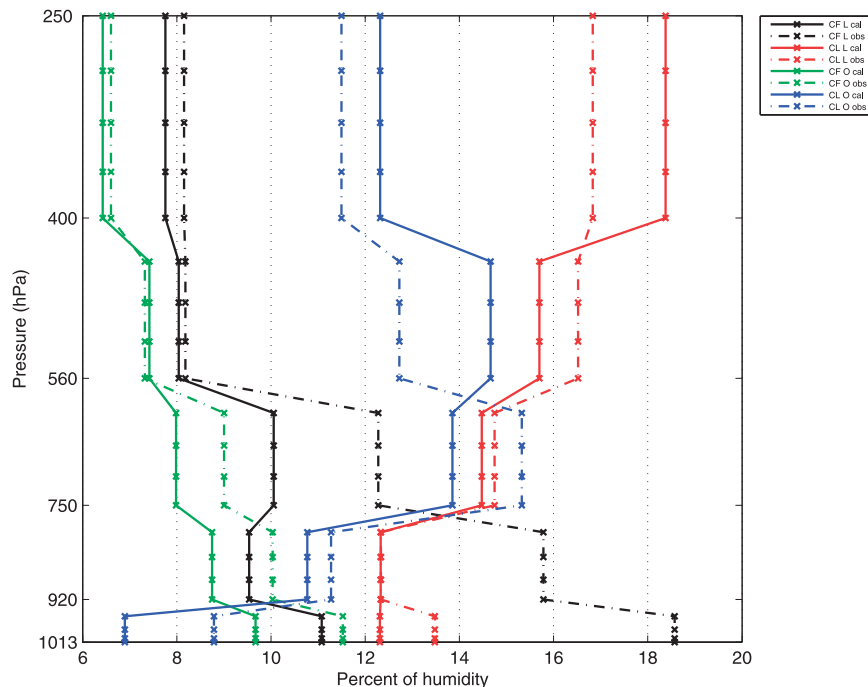


FIG. 5. RMS relative humidity departure of the ECMWF analysis and the retrieval from raw (dotted) and calibrated (solid) *Aqua* observations for cloud free/land (black), cloudy/land (green), cloud free/ocean (red), and cloudy/ocean (blue) configurations.

Figure 8 represents the RMS errors between RTM simulations and satellite observations (calibrated or not). The four configurations are considered: cloud free over ocean scenes, cloud free over land scenes, cloudy over ocean scenes, and cloudy over land scenes. The different colored curves are explained here:

Green curve = $\text{RMS RT}(\text{ana}) - \text{obs}$: “distance” between the analysis and the satellite observations. Any improvement relative to this curve means that the retrievals improve the analysis by getting closer to the satellite observations.

Purple curve = $\text{RMS RT}[\text{INV}(\text{obs})] - \text{CAL}(\text{obs})$: quality of the retrieval when using noncalibrated data for the inversion.

Red curve = $\text{RMS RT}(\text{ana}) - \text{CAL}(\text{obs})$: level of agreement between the analysis and the satellite observations. It is legitimate to compare the TB simulations with calibrated observations because the calibration procedure has been designed based on these analyses. As a consequence, the agreement is always improved relative to the comparison with raw observations (i.e., green curve).

Blue curve = $\text{RMS RT}[\text{INV}(\text{obs})] - \text{obs}$: remaining discrepancies when the retrieval is performed on noncalibrated observations. This statistic is represented here to allow for comparisons of

third-party retrieval statistics using no calibration procedure.

Black curve = $\text{RMS RT}\{\text{INV}[\text{CAL}(\text{obs})]\} - \text{CAL}(\text{obs})$: internal coherency of the retrieval scheme (including the calibration step). The whole inversion process consists of minimizing their sum over the channels.

Dealing with all these statistics can be confusing, but the comparison of these curves allows us to measure different quantities. For example, the comparison of the green and purple curves shows that even if no calibration is used, the inversion process globally improves the analysis.

When the purple and the black curves are compared, the calibrated observations are chosen as the reference. This makes sense because we are using a physical retrieval scheme and the inherent assumption is that the RTM is reliable. The comparison of these two curves measures the direct impact of the calibration on the quality of the retrievals. The differences can reach a few degrees and are highly significant for the four configurations and all channels, especially the channels with large errors before calibration. For several channels, most of them in H polarization, the RMS error is divided by 2 or more.

The comparison of the blue and black curves estimates the improvement offered by the proposed calibration step when correcting systematic RTM and NWP

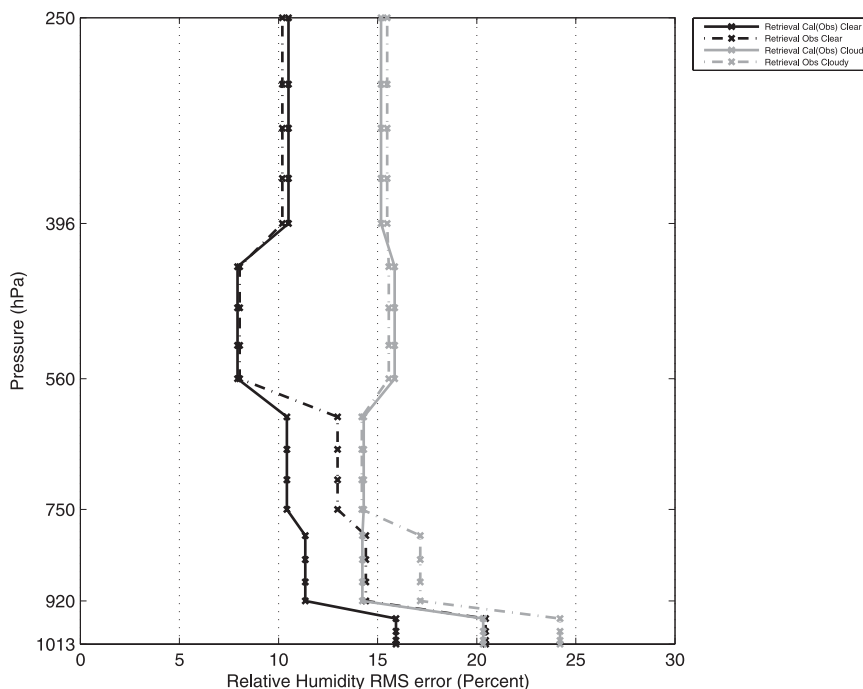


FIG. 6. RMS differences in relative humidity between a collection of radiosonde measurements and coincident retrievals from raw (dot-dashed) and calibrated (solid) *Aqua* observations. These statistics are performed over land for clear (gray) and cloudy (black) scenes over two months over the tropics.

errors. It shows that the retrieval scheme is much more coherent when performed in the calibrated data space than in the direct observation space. This means that the mathematical process of the inversion is more robust in the “regularized” space of the calibrated satellite observations space.⁴

The difference between the black and red curves demonstrates that the analysis has been improved, even in the space of the calibrated satellite observations. It is legitimate to do this comparison on the calibration data space because the calibration process has been trained on the analysis; in a similar way, it helps the analysis and the retrievals. This improvement would also be observed if compared with direct noncalibrated observations (not shown).

5. Discussion

For purposes of clarity, it is helpful to return to the definition and the goal of the calibration in this study.

⁴ The inversion of satellite observations is often an ill-posed problem, and many mathematical techniques tend to regularize the problem. Transforming the input or output data by “projecting” them in spaces where the inversion is better constrained is a classical approach (Tarantola 1987).

Calibration of a satellite instrument means quantifying its responses to known signals that are traceable to agreed standards. This is based on the assumption that the standard is stable and more reliable than the satellite instrument. However, in the context of this paper, it is arguable whether the agreed “reference” dataset, the ECMWF analysis with RTTOV simulations, is any better known than what the satellite responses to signals are. In fact, the satellite instrument calibration today has accuracies better than 1 K, so the large biases between observations and simulations presented in Table 1 cannot be totally attributable to satellite observations; some is due to errors in the NWP and RTM models. It should be clear here that the goal of the NN calibration procedure is not to perform an absolute calibration of the *Aqua* instruments. The goal is to compensate for these NWP and RTM model errors as a preprocessing step before the retrievals. It has been shown in previous sections that the use of the NN calibration procedure improves the inversions.

This preprocessing approach competes with methods that train a single retrieval NN to match observed radiances to a real-time NWP model. The proposed two-step NN method is important primarily when an operational NWP model used for training and operations is effectively less accurate than the offline NWP model used for

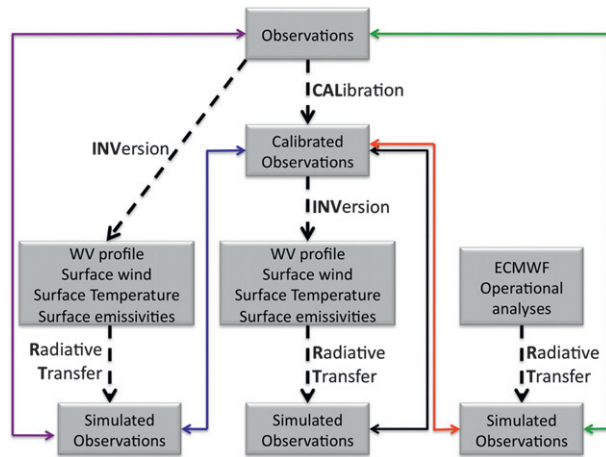


FIG. 7. Validation scheme for TB space. Processes are represented with thick and dashed black arrows; comparisons of the TB space are represented with double arrows (colors are as in Fig. 8).

training because of real-time misalignment of data in space or time or unknown surfaces. Misalignment errors, for example, include those associated with rapidly moving sharp water vapor fronts.

The main limit to the NN calibration procedure presented here is that NWP and RTM errors often vary in time and space in complex ways. The NN approach is nonlinear and its behavior is state dependent but the errors might not be fully revealed by the raw radiances only. This suggests that one way to improve the method is to include, as input with the raw radiances, all available relevant prior information that does not compromise the result (e.g., scan angle, season, latitude, surface type, elevation), provided that the training dataset is sufficiently large that the enlarged network does not become unstable. This will be the subject of forthcoming developments.

The proposed calibration procedure for inversion using an NN model is very general and could be used for various calibration problems related to remote sensing applications. For example, the method can place data from multiple satellites on a single footing. First, the

“reference” dataset on which the raw observations are “projected” can be, again, RTM simulations on NWP analysis. In this approach, the calibration will benefit directly any retrieval scheme that is based on the NWP and RTM models. The instruments can be different, with different observing channel characteristics. Second, the reference dataset can also be one of the instrument raw observations. This approach would necessitate putting into spatiotemporal coincidence the two sets of observations: the NWP + RTM errors would not factor into this configuration, but coincidence errors would be introduced. This scheme is particularly appropriate for cases in which the instruments have similar characteristics: the instruments can have slightly different characteristics, but in this case the calibration could operate only on the common information content part of the observations.

Another application of the proposed NN scheme is the time calibration of satellite measurements to limit instrument drift. As always, a reference dataset needs to be defined. Again, the first solution is that it can be based on NWP analysis, but only if the instrument observations have not been assimilated in the analysis. In the second solution, the reference data can also be an ensemble of RTM simulations performed on radiosonde measurements. In this case, the radiosonde ensemble must be diversified (e.g., air mass, latitude, surface type, viewing angle of the satellite observations in coincidence) with a quite constant measurement network over time. This is a true challenge, of course. An adaptive training algorithm based on these evolving radiosonde measurements can be employed to modify over time the behavior of the NN calibration scheme in order to obtain a time-drift correction. When a retrieval algorithm is developed, it is often validated using radiosonde measurements. Significant bias between retrievals and the in situ measurements can be observed and a calibration method can be used as a postprocessing step to reduce them. The NN calibration procedure proposed in this study can also be used in this context and will benefit, again, from its multivariate and nonlinear capacities.

TABLE 2. Explanation of the data components used in the TB space validation: CAL is calibration, INV is inversion (i.e., RTM^{-1}), RT is radiative transfer, and ANA is the ECMWF analysis.

Name used in the text	Processing chain	Description
Obs	...	Raw observation
CAL(obs)	obsCAL ...	Calibrated observations
INV(obs)	obsINV ...	Retrieval performed on raw (observations)
INV[CAL(obs)]	obsCAL ... INV ...	Retrieval performed on calibrated (observations)
RT[INV(obs)]	obsINV ... RT ...	Radiative transfer done on INV(obs)
RT{INV[CAL(obs)]}	obsCAL ... INV ... RT ...	Radiative transfer done on {INV[CAL(obs)]}
RT(ana)	anaRT ...	Radiative transfer done on NWP(analysis)

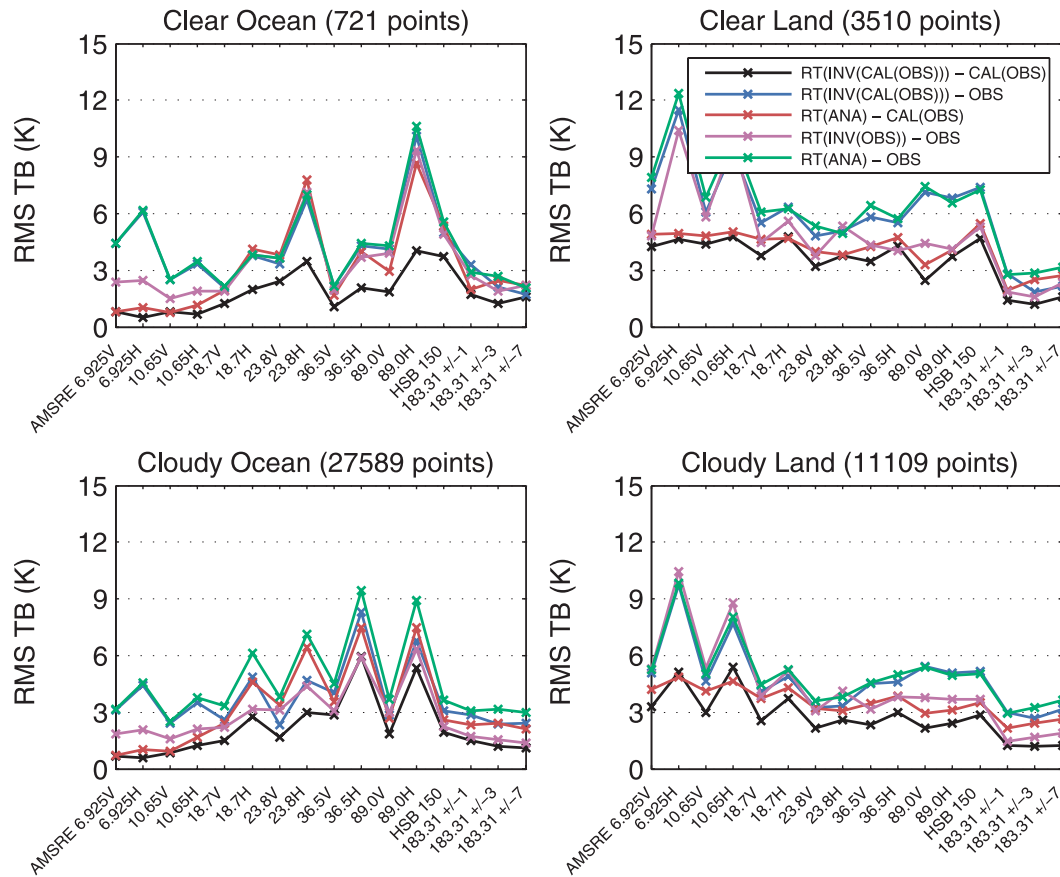


FIG. 8. RMS differences between RTM simulations and calibrated (or noncalibrated) real observations. The RMS errors are for RT(ana) – obs (green), RT[INV(ana)] – CAL(ana) (purple), RT(ana) – CAL(ana) (red), RT[INV(ana)] – OBS (blue), and RT{INV[CAL(ana)]} – CAL(ana) (black). See the text and Table 2 for explanations.

The NN calibration methodology can also be used to compensate for failing channels. Let m be the number of channels in the instrument. For each missing channel, an NN calibration model can be trained from the initial $(m - 1)$ -dimensional space of raw channels to the m -dimensional space of calibrated channels. These m models perform a spectral interpolation to generate a synthetic measurement that can replace the failing channel. This is possible because there are strong correlations among the observing channels. This very simple scheme would allow the use of an already implemented retrieval algorithm without any significant modification.

6. Conclusions

In this paper, a novel calibration procedure based on neural networks is presented. This NN calibration is satisfactory: it reduces the differences between observed and simulated TBs and, as a consequence, the retrieval scheme performs better on the calibrated observations.

An experiment has been conducted on real AMSR-E/HSB observations on board the *Aqua* platform: the retrieval of WV has been improved by the use of the calibration scheme. This test also illustrated two additional important facts:

- 1) It is now possible to simulate quite realistically satellite observations over continental surfaces, and retrieval can be performed well over land when realistic surface emissivities are adopted (Aires et al. 2001; Karbou et al. 2005); and
- 2) The presence of nonprecipitating clouds can be adequately accounted for in the retrieval process (Chevallier and Bauer 2003).

This calibration procedure is very general and could be used in different contexts such as

- to intercalibrate instruments from different platforms (e.g., for satellite constellations such as the Global Precipitation Measurement missions),

- to calibrate retrieval products toward in situ measurements, and
- to perform adaptive calibration to reduce the impact of instrument drifts during their lifetime.

The methodology can also be used as an attractive and efficient way to solve the problem of a failing channel: The calibration model performs a spectral interpolation to generate a synthetic channel measurement that can replace the failing measurement, allowing the use of an already implemented retrieval algorithm without any significant modification.

The perspectives of this work are to extend the calibration process to other satellites, in particular for the AMSU-A, AMSU-B, and MHS instruments on board the MetOp platform or the Saphir and Madras instruments on board the Megha-Tropiques mission. These calibration procedures have been developed to build retrieval chains for these platforms. We would also like to test the addition of external information in the scheme, such as surface type or air mass.

Acknowledgments. This work has been performed in the framework of the development of the algorithms for the Megha-Tropiques mission, with the Centre National d'Etudes Spatiales (CNES) support. Megha-Tropiques is a French–Indian satellite to be launched in 2011. Its objective is to study the water cycle in the tropics, with a high temporal sampling. It will carry two microwave instruments, a conical imager, Madras, and a cross-track humidity sounder, Saphir. We are particularly grateful to Didier Renaut from the CNES, for his involvement in this study. We thank Rémy Roca for interesting discussions related to the Megha-Tropiques mission. We thank Nicolas Viltard and Sonia Labetoule for providing a cross-track/conical coincidence code. We are also grateful to the ARA group at LMD for providing their radiosonde database.

REFERENCES

- Aires, F., and C. Prigent, 2007: Sampling techniques in high-dimensional spaces for satellite remote sensing database. *J. Geophys. Res.*, **112**, D20301, doi:10.1029/2007JD008391.
- , —, W. Rossow, and M. Rothstein, 2001: A new neural network approach including first guess for retrieval of atmospheric water vapor, cloud liquid water path, surface temperature, and emissivities over land from satellite microwave observations. *J. Geophys. Res.*, **106** (D14), 14 887–14 907.
- Blum, A., and R. Rivest, 1992: Training a three-node neural network is NP-complete. *Neural Networks*, **5**, 117–127.
- Brest, C., W. Rossow, and M. Roiter, 1997: Update of radiance calibrations for ISCCP. *J. Atmos. Oceanic Technol.*, **14**, 1091–1109.
- Brogniez, H., R. Roca, and L. Picon, 2006: A clear-sky radiance archive from Meteosat water vapor observations. *J. Geophys. Res.*, **111**, D21109, doi:10.1029/2006JD007238.
- Chevallier, F., and P. Bauer, 2003: Model rain and clouds over oceans: Comparison with SSM/I observations. *Mon. Wea. Rev.*, **131**, 1240–1255.
- Colton, M., and G. Poe, 1999: Intersensor calibration of DMSP SSM/I's: F-8 to F-14, 1987–1997. *IEEE Trans. Geosci. Remote Sens.*, **37**, 418–439.
- Cybenko, G., 1989: Approximation by superpositions of a sigmoidal function. *Math. Control Signals Syst.*, **2**, 303–314.
- Deblonde, G., and S. English, 2001: Evaluation of the FASTEM-2 fast microwave oceanic surface emissivity model. *Tech. Proc. ITSC-XI*, Budapest, Hungary, WMO, 67–78.
- Eyre, J., 1991: A fast radiative transfer model for satellite sounding systems. ECMWF Research Dept. Tech. Memo. 176, 28 pp.
- Gutman, G., 1999: On the use of long-term global data of land reflectances and vegetation indices from the advanced very high resolution radiometer. *J. Geophys. Res.*, **104**, 6241–6255.
- Hornik, K., M. Stinchcombe, and H. White, 1989: Multilayer feedforward networks are universal approximators. *Neural Networks*, **2**, 359–366.
- Karbou, F., F. Aires, C. Prigent, and L. Eymard, 2005: Potential of Advanced Microwave Sounding Unit-A (AMSU-A) and AMSU-B measurements for atmospheric temperature and humidity profiling over land. *J. Geophys. Res.*, **110**, D07109, doi:10.1029/2004JD005318.
- Kawanishi, T., and Coauthors, 2003: The Advanced Microwave Scanning Radiometer for the Earth Observing System (AMSR-E), NASA's contribution to the EOS for global energy and water cycle studies. *IEEE Trans. Geosci. Remote Sens.*, **41**, 184–194.
- Lambrigtsen, B., and R. Calheiros, 2003: The humidity sounder for Brazil: An international partnership. *IEEE Trans. Geosci. Remote Sens.*, **41**, 352–361.
- Matricardi, M., F. Chevallier, and S. Tjemkes, 2001: An improved general fast radiative transfer model for the assimilation of radiance observations. ECMWF Research Dept. Tech. Memo. 345, 42 pp.
- Picon, L., R. Roca, S. Serrar, J. Monge, and M. Desbois, 2003: A new Meteosat “water vapor” archive for climate studies. *J. Geophys. Res.*, **108**, 4301, doi:10.1029/2002JD002640.
- Prigent, C., W. Rossow, and E. Matthews, 1997: Microwave land surface emissivities estimated from SSM/I observations. *J. Geophys. Res.*, **102**, 21 867–21 890.
- , F. Aires, and W. Rossow, 2006: Land surface microwave emissivities over the globe for a decade. *Bull. Amer. Meteor. Soc.*, **87**, 1573–1584.
- , E. Jaumouille, F. Chevallier, and F. Aires, 2008: A parameterization of the microwave land surface emissivity between 19 and 100 GHz, anchored to satellite-derived estimates. *IEEE Trans. Geosci. Remote Sens.*, **46**, 344–352.
- Rossow, W., and R. Schiffer, 1999: Advances in understanding clouds from ISCCP. *Bull. Amer. Meteor. Soc.*, **80**, 2261–2287.
- Rumelhart, D., G. Hinton, and R. Williams, 1986: Learning internal representations by error propagation. *Parallel Distributed Processing: Explorations in the Microstructure of Cognition*. D. Rumelhart and J. McClelland, Eds., MIT Press, 318–362.
- Saunders, R., M. Matricardi, and P. Brunel, 1999: An improved fast radiative transfer model for assimilation of satellite radiance observations. *Quart. J. Roy. Meteor. Soc.*, **125**, 1407–1425.

- Tarantola, A., 1987: *Inverse Problem Theory: Models for Data Fitting and Model Parameter Estimation*. Elsevier, 630 pp.
- Uppala, S., and Coauthors, 2005: The ERA-40 re-analysis. *Quart. J. Roy. Meteor. Soc.*, **131**, 2961–3012.
- Weng, F., B. Yan, H. Xu, and N. Sun, 2005: Assessment of DMSP series of SSM/I data for NOAA weather and climate applications. *Proc. SSMIS Working Group Meeting*, Monterey, CA, SSMIS, 21 pp.
- Zou, C.-Z., M. D. Goldberg, Z. Cheng, N. C. Grody, J. T. Sullivan, C. Cao, and D. Tarpley, 2006: Recalibration of microwave sounding unit for climate studies using simultaneous nadir overpasses. *J. Geophys. Res.*, **111**, D19114, doi:10.1029/2005JD006798.
- , M. Gao, and M. D. Goldberg, 2009: Error structure and atmospheric temperature trends in observations from the Microwave Sounding Unit. *J. Climate*, **22**, 1661–1681.